공학석사 학위논문

Dye Molecule Additive Engineering for Enhanced Properties of Perovskite Solar Cells

염료 첨가제를 이용한 페로브스카이트 태양전지의 성능 향상 연구

2020년 2월

서울대학교 대학원

재료공학부

홍 인 화

Abstract

Dye Molecule Additive Engineering for Enhanced Properties of Perovskite Solar Cells

Inhwa Hong

Department of Materials Science and Engineering

The Graduate School

Seoul National University

Organic-inorganic halide perovskite solar cells have passed PCE of 25% and been studied to reach the Shockley-Queisser efficiency limit efficiency. However, the stability issues of the device are still unsolved and many approaches have been conducted. The unsatisfied stability is mainly due to the poor and unstable crystallinity, caused by ionic defects in perovskite layer. To date, tremendous numbers of studies have done on improving the crystallinity. Dye

molecule additive is considerable and effective way to enhance the crystallinity. The substituents, especially negatively charged functional group, might coordinate to the metal cation defects caused by I^- vacancy. Herein, we demonstrated the enhanced properties of $MAPbI_3$ perovskite with D35CPDT molecule additive, which leads to increase in photovoltaic performances. The size of the grains, crystallinity, optical absorptions, and carrier life time increased with the addition of D35CPDT molecule in the perovskite precursor. These enhancements increased the current density (J_{sc}) from 21.06 mA cm^{-2} to 22.06 mA cm^{-2}, ultimately increased the power conversion efficiency from 17.48 % to 18.56 %. Moreover, we discuss the improved stability of the photovoltaic devices with dye additives. The current density (J_{sc}) and the open-circuit voltage (V_{oc}) of $MAPbI_3$ with D35CPDT molecule additive remained more than 80% after 650 hours kept in ambient without encapsulation, while those for reference dropped to 0 % after 650 hours. This observation can give insight that addition of large molecule with functional group and alkyl groups can not only improve the perovskite crystallization properties, but also can elongated the lifetime of the devices.

Keywords: Perovskite solar cell, Solution Process, Additive Engineering, Defect Passivation, Molecular additives

Student Number: 2018-29417

Table of Contents

List of Tables

List of Figures

Chapter 1. Introduction

1.1 Recent Researches and Developments in Perovskite Solar cells

Since the first generation silicon-based solar cells were introduced to the world, photovoltaics has attracted great attention as substitutes for fossil fuel. Among them, the organic-inorganic halide perovskite solar cells have brought remarkable improvements in performances with the efficiency exceeding 25% [1] from an initial power conversion efficiency of 9.7% [2]. It is believed that the perovskite is promising material for next-generation photovoltaics, due to its many intriguing advantages, such as easily tunable band-gap [3,28,51], low exciton binding energy [4, 29,55], and high carrier mobility [5,30,54], high absorption coefficient [6, 31] , and long carrier diffusion lengths [7,32].

However, while the high efficiency of device has been achieved rapidly, there is still continuing issues in unsatisfied stability [8]. The ionic materials such as organic-inorganic halide perovskite have considerable quantity of under-coordinated ions. [33] Especially the I^- vacancy, the main migration species, can migrate into perovskite grains [9], and drift toward perovskite-metal electrode leading to the corrosion of metal electrode. [34-36] This phenomenon can induce a lot of defects in the perovskite film, which will accelerate the degradation of perovskite films. [10,51-53] These defects tend to be formed at the surfaces and grain boundaries of perovskite film, which can serve as non-radiative recombination center decreasing the charge carrier lifetime and leading poor the device performances. [11,37] In addition, defect trap states and grain boundaries are vulnerable to moisture or oxygen. [12,13,38]

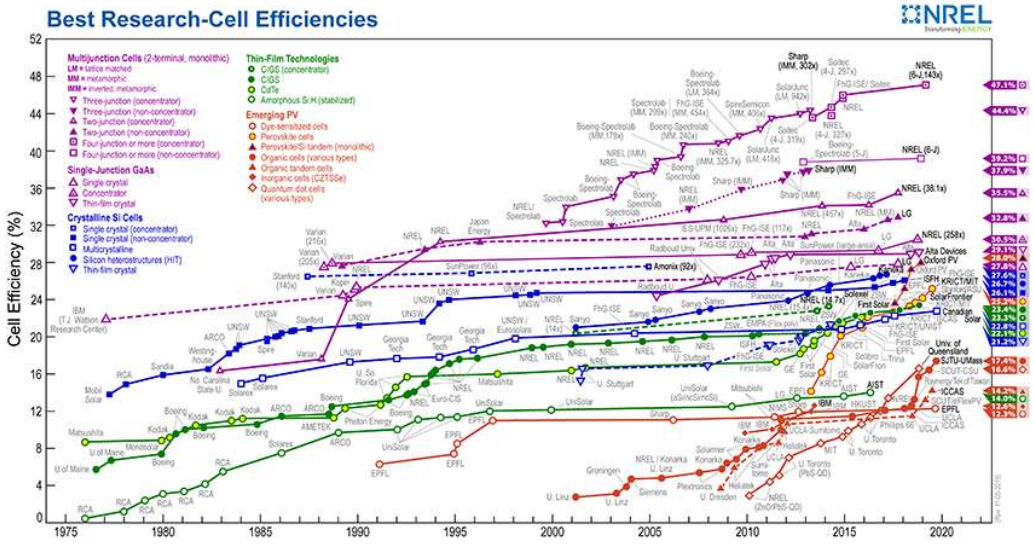

Figure 1.1.1 The latest chart on record solar cell efficiencies. [1]

1.2 Additive engineering

Various demonstrations on the passivation of I^- vacancy defects were proposed by adding excess amount of iodine species in the perovskite precursor. [26,40-42] Adding excess amount of iodine without involving the A-site substitution allowed only the additive candidates to be methyl ammonium Iodide (MAI) and lead(II) Iodide (PbI_2). [14, 26] The I^- vacancy would be passivated by the excess amount of I in the additives, but this can lead another defects due to the excess amount of MA^+ or pb^{2+}. [27,39-42] Thus, other benign anion additives were required and a little of researches on dye as the additive of the perovskite have been conducted. [15] In most of organic dyes, Carboxyl group (-COOH) is linked to flexible carbon chain, which usually makes strong coordination to metal cations such as Pb^{2+}. [15,43-47] The hydrophobic alkyl chains in dye molecules can act as a moisture barrier and improve the stability as well. [15,43-47] Therefore, the dyes can be expected to be promising candidates of additives for perovskite materials.

In this study, we have chosen D35CPDT, which is composed with cyclopentadithiophene linker unit, hexyl chains, and carboxylic acid. [16] According to the research done on D35 type donor dye by Erik Gabrielsson et al, D35CPDT is huge advantageous for achieving high extinction coefficient as the linker is essentially locked in a planar conformation. [16, 17] We assumed that each functional group on this dye molecule might passivate the I^- vacancy by coordinating with Pb^{2+}. [48-50] We successfully demonstrated that the D35CPDT dye molecule additives effect on optical properties of $MAPbI_3$ perovskite films with improved crystallinity and increased morphology. In particular, the addition of the dye additives significantly improves the optoelectronic properties and carrier life time of perovskite film. As a result, the $MAPbI_3$ perovskite solar cell with D35CPDT dye molecule exhibited improved photovoltaic performances and stability.

Chapter 2. Experimental Details

2.1 Device Fabrication

The schematic of dye fabrication is given in the Figure 2.1.1. The ITO/glass substrates in 2 cm* 2 cm size were washed with detergent solution, deionized water and Isopropanol for 5 minutes each in sonicator bath, and dried with dry nitrogen. The cleaned substrates were treated with UV-ozone for 15 minutes before use to increase the wet-ability.

Methylammonium Iodide (MAI) and Lead (II) Iodide (PbI_2) (1:1 molar ratio) were dissolved in anhydrous *N,N*-dimethylformamide (DMF) : Dimethylsulforxide (DMSO) (9:1 v/v%) mixture to make 1.5 M of perovskite precursor solution. The precursor solution was stirred for more than 2 h at room temperature in Nitrogen-filled glovebox. For the D35CPDT was dissolved in same DMF: DMSO solvents, followed by a sufficient dissolving for over 24 h. The dye molecule additive was directly added to perovskite precursor from pre-made stock solution with various concentration: 0, 6.0 $e^{-5,}$ and $2.0e^{-4}$ M. The $MAPbI_3$ with D35CPDT molecule additive was denoted as LC dye and HC dye for lower concentration and higher concentration, respectively. Hole transporting layer (HTL) was prepared by dissolving 25 mg of Nickel (II) Acetate Tetrahydrate in 1 ml of anhydrous ethanol for more than 30 mins and filtered before use. NiO_x was spin-coated on cleaned ITO substrates at 4000 r.p.m. for 40s, and the films were immediately annealed at 300 ^oC for 3 h. After cooling, the HTL coated substrates were transferred to a nitrogen filled glovebox, and the perovskite precursor was spin-coated at 4,000 r.p.m. for 25s. During the spin-coating, anhydrous diethyl ether was rapidly poured onto the spinning substrates. The perovskite films were immediately annealed for 1 min at 65^oC, and then 30 mins at 100^oC on preheated hot plates. After cooling down, [6,6]-phenyl-C_{60}-Butryic acid methyl ester ($PC_{60}BM$) solution (25 mg mL^{-1} in 1,2-dichlorobenzene) was spin-coated on the perovskite layer at 6000 r.p.m. for 60 s. Diluted PEIE was spin-coated on top of PCBM

at 6,000 r.p.m. for 30s. Then, the samples were taken from the glovebox and finished by thermally evaporating Ag electrodes through a patterned shadow mask under a vacuum.

For perovskite film only samples were deposited on cleaned ITO/glass substrates or soda lime glasses, with same method used for the device fabrication.

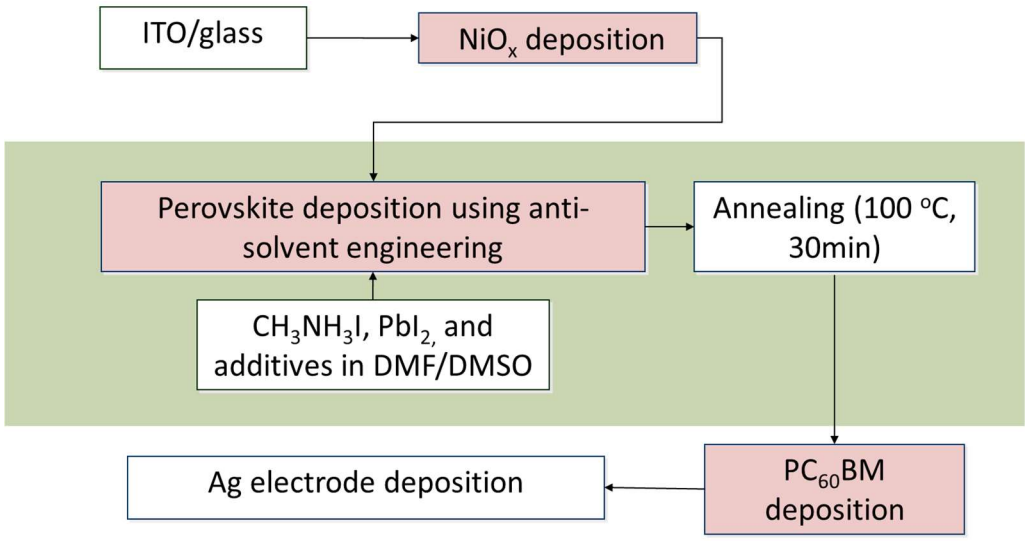

Figure 2.1.1. Schematic device fabrication of perovskite solar cell.

2.2 Characterization

The optical properties of samples and solutions, such as their absorption spectra, were measured with Ultraviolet-Visible-Near-Infrared spectrophotometer (Cary5000, Agilent). Field-emission Scanning Electron Microscopy (FESEM; JSM-7600F, JEOL) was used to observe the morphology and thickness of perovskite film on ITO substrates. Photoluminescence spectra was obtained by spectrofluorometer (PicoQuant, FlouTime 300). The existence of D35CPDT molecule was studied with ToF-SIMS depth profiling (ToF.SOMS-5, ION-ToF). The crystal structures of perovskite films with and without two different concentrations were confirmed using X-ray diffraction measurement (XRD; New D8 Advance, Bruker) using Cu Kα radiation (λ=0.1542 nm). External Quantum Efficiency (EQE) spectra was recorded using 4-Hz-chopped monochromatic light without light or potential bias (EQE; QUANTX-300, NEWPORT).

For the Electrochemical Impedance Spectroscopy (EIS) measurements, the device was illuminated using white LED lamp (Thorlabs MWWHLP1) was measured under 1-sun with bias voltage of V_{oc}.

The light current density-voltage (*J-V*) characteristic was obtained by potentiostat under AM 1.5G solar irradiation generated using solar simulator. The devices were masked with a metal aperture to define an active areas of 0.14 cm^2.

Chapter 3. Results and Discussion

The perovskite film was fabricated according to the all-solution anti-solvent process in this study. [39,40] Generally, in all-solution anti-solvent process, the additive engineering can be conducted by adding the additive straight into precursor solutions or by pouring the additive dissolved in anti-solvents onto the precursor film during spin-coating. However, the selective solubility of D35CPDT, the additive used in this study, lead the additive to be insoluble in non-polar solvent such as anhydrous diethyl ether [18] and toluene which are commonly used in anti-solvents process. Due to the very low solubility of this dye, we adopt the former method.

3.1 Dye Molecules as Additives

3.1.1 Introduction of dye molecule as additives

Before perovskite material started to be paid attention, dye-sensitized solar cells (DSSCs) were actively studied due to its simple synthetic methods, flexible stereochemical configurations, and good stability. [19] As perovskite solar cells is developed from DSSCs, there have been several attempts on selecting dye molecules as defect passivators in perovskite solar cells for their many advantages that were proved in dye-sensitized. Li et el. Had employed AQ301 dye molecule as trap state passivator and proved the increased stability. [19] Zhang et el. Suggested N719 dye molecule as efficient additive for improving moisture stability. [20] Even though the dyes can be expected to be promising candidates of additives for perovskite materials, a little of researches on dye as the additive of the perovskite have been conducted. In this studies, total of 5 different dye candidates were chosen in order to studies in this research. The structures of dye molecule are depicted in Figure 3.1.1. Among those candidates, Z907, N3, N749, and N719 are organic-metal dyes and D35CPDT is organic dye. All the candidates are consisted with one or more

functional groups, such as carboxyl group, which usually makes strong coordination to metal cations such as Pb^{2+}.

3.1.2 Characterization of Perovskite film with and without dye molecule additive

All of the dye candidates are soluble in polar aprotic solvent, they were dissolved in DMF/DMSO mixture which is the polar aprotic solvent system for perovskite precursor at each concentration of $6.0e^{-5}$. The colour of solutions changed as shown in Figure 3.1.2, as the pre-dissolved dye solutions were directly added into $MAPbI_3$ precursor solutions. The color changes of the precursor solutions from yellow to coral, green, or purple depending on which dye is added.

Several optical analyses, such as UV-Vis spectroscopy and Photoluminescence (PL) on spin-coated $MAPbI_3$ films with or without dye additives were demonstrated in order to scan dye molecules as efficient additives. First, the UV-Vis absorption spectra of $MAPbI_3$ solution and films with or without dye additives were exhibited in Figure 3.1.3. To evaluate the charge transport properties of the perovskite-dye films, we performed stead-state photoluminescence (SSPL) and time-resolved PL measurements, as shown in Figure 3.1.4. The SSPL intensity achieved maximum in the perovskite with dye molecule mixture incorporated perovskite films on glass. The higher PL intensity implies that a moderate amount of D35CPDT incorporation could improve the crystallinity ad reduce defects. Decreased SSPL intensity at the Perovskite with N749 hybrid film can be attributed to the poor crystal quality of the perovskite films as indicated by the XRD results. Perovskite films with SSSS show a slower PL decay corresponding to a longer lifetime. This suggests that D35CPDT modification is effective in reducing non-radiative recombination in perovskite films, which can be attributed to improved crystal growth and defect passivation.

Along with former analysis, X-ray Diffraction analysis was also conducted to observe changes in physical properties. As shown in Figure 3.1.5, intensities of the (110), (220), and (310) peak were increased as the dye is added into the control solution. Intensity of each peaks in XRD analysis indicates the quantity of the grains in the film. There proves that there are improvements in both optical and physical properties of perovskite with dye molecule addition.

These perovskite solar cells with and without due candidates were also examined in order to scan the device performances. All four parameters are depicted in Figure 3.1.6. Along with the optical analysis, the device performances data indicates that the D35CPDT is the best candidates for further studies. The effect of D35CPDT dye molecule engineering will be further discussed in later sections.

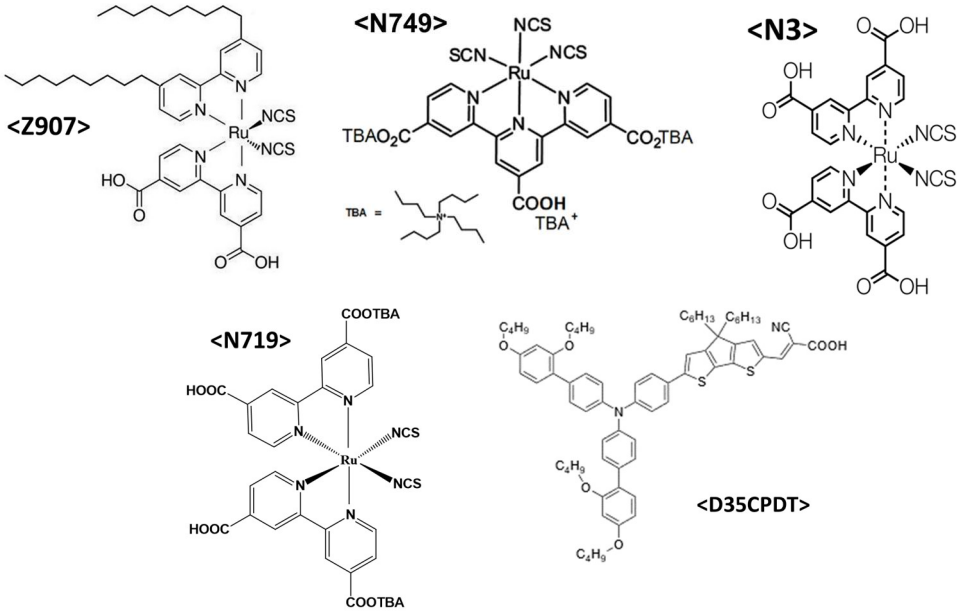

Figure 3.1.1. Structures of dye candidates.

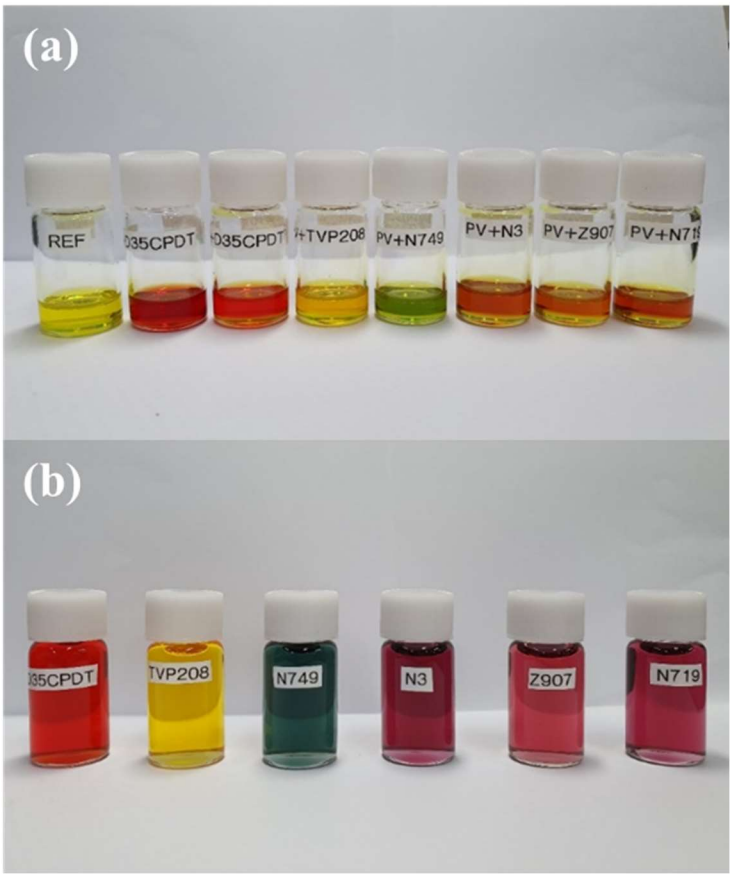

Figure 3.1.2. Image of (a) Perovskite precursor $MAPbI_3$ solution and perovskite with dyes molecule additives ($6.0e^{-5}$M), (b) Dye Stocks.

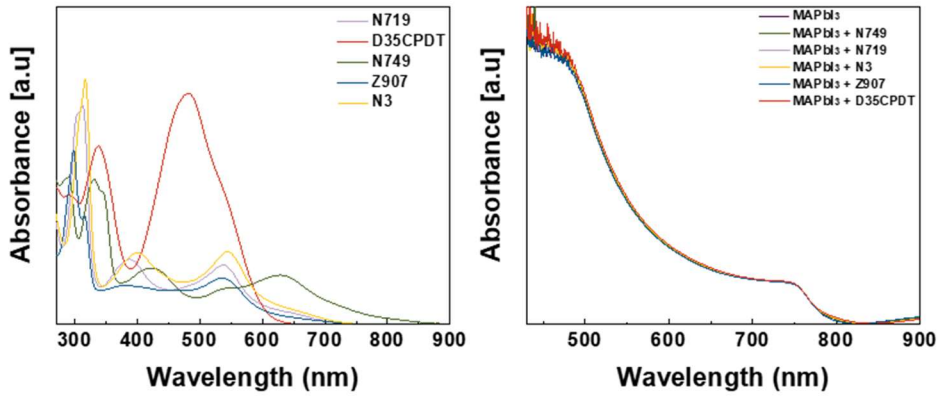

Figure 3.1.3. UV-Vis absorption spectra of dye solutions (left) and $MAPbI_3$ films with or without dye (right).

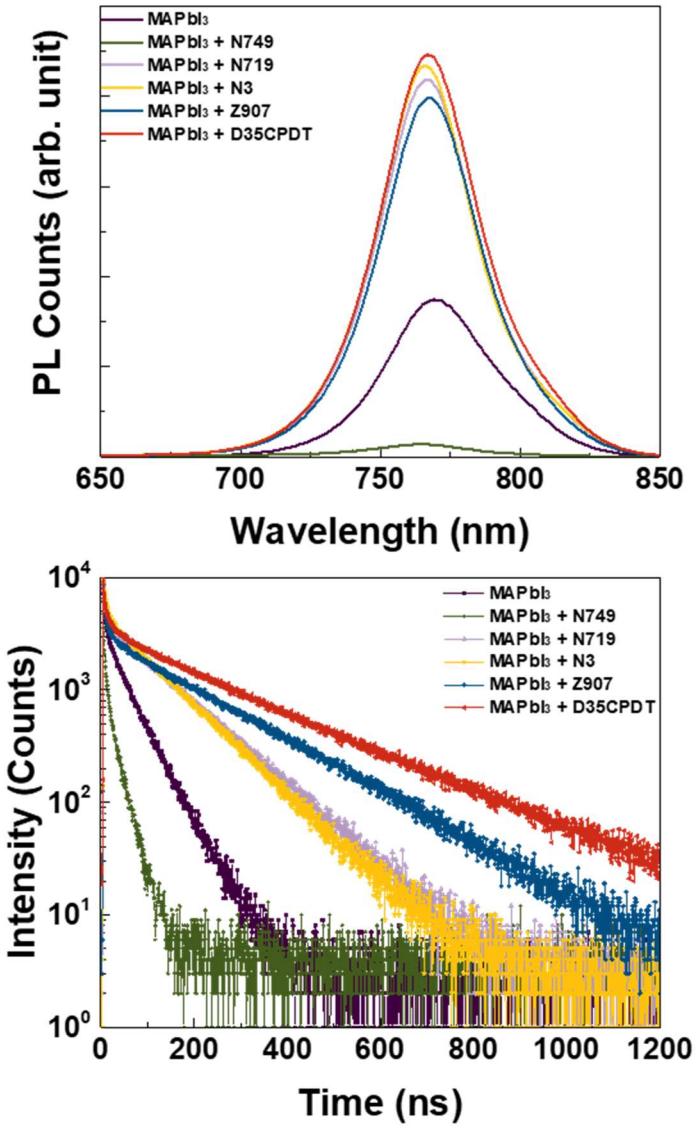

Figure 3.1.4. Photoluminescence (PL) spectra of dye solutions PL spectra of the perovskite layer with different dye (Top) Steady-state and (Bottom) transient-state.

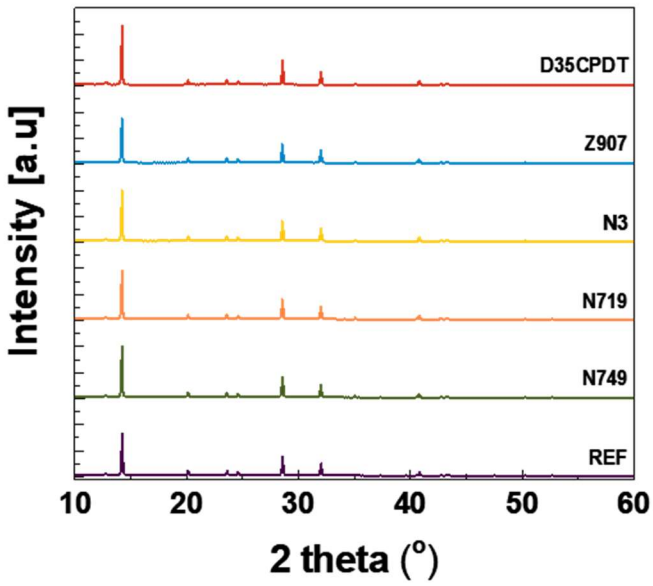

Figure 3.1.5. XRD patterns for various dyes containing perovskite films.

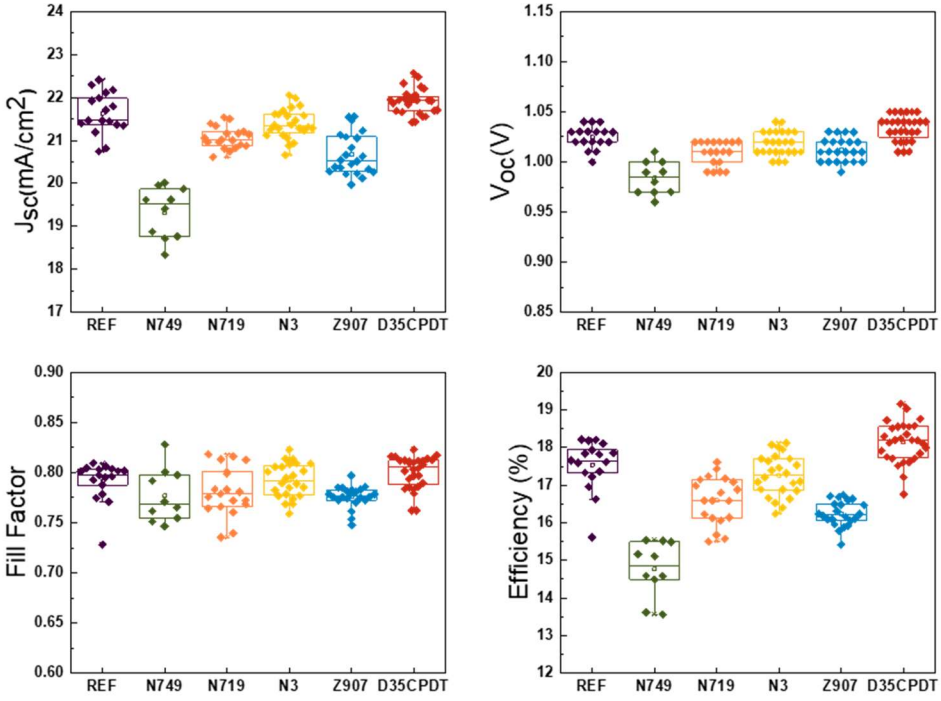

Figure 3.1.6. Photovoltaic parameters a) J_{sc} (mA/cm2), b) V_{oc} (V), c) Fill factor, and d) Efficiency (%) of perovskite solar cells with different dyes.

3.2 Characterization of D35CPDT Molecule Additive Engineering

3.2.1 Optical Properties of Perovskite film with and without D35CPDT molecule additive

The structure of the D35CPDT dye is illustrated in Figure 3.2.1 (a). This D35CPDT dye is soluble in polar aprotic solvent, so the D35CPDT dye powder was dissolved in DMF/DMSO mixture which is the polar aprotic solvent system for perovskite precursor at each concentration of $6.0e^{-5}$M and $2.0e^{-4}$M. The D35CPDT dye solutions were added directly to $MAPbI_3$ precursor solutions and denoted as LC dye and HC dye for lower concentration and higher concentration, respectively. The dye-free perovskite film fabricated using only $MAPbI_3$ was prepared for comparison and denoted as reference. The images of $MAPbI_3$ solutions with or without D35CPDT dye additive, and D35CPDT stock solution are shown in the Figure 3.2.1 (b). Even though the concentrations of D35CPDT dye additive are very low, we clearly observed the color change of the precursor solutions from yellow to coral-yellow as the dye solution was added into the precursor solution due to the color of D35CPDT dye. The light absorption of perovskite films is one of the critical precognition parameter in terms of achieving high performance solar cell. Therefore, we first performed UV-Vis spectroscopic analysis to examine any optical changes due to dye molecule addition. The UV-Vis absorption spectra of $MAPbI_3$ films with and without LC dye and HC dye additives were exhibited in Figure 3.2.1. Compared to the absorption spectrum of reference perovskite film, the overall shape of UV-Vis absorption spectra for perovskite films with dye additives remained intact without any shift. The maximum absorption wavelength, $\lambda_{max,1}$ and $\lambda_{max,2}$, of D35CPDT solution were measured at 337 nm and 483 nm, respectively Figure 3.2.2., but there is only negligible change of absorption

intensity at the above mentioned wavelengths in the annealed perovskite film incorporated by dye. The absolute light absorption intensity increased in overall range from 450nm to 820nm, while the specific enhancement at the dye's maximum absorption wavelength was not observed. This observation explains that the D35CPDT does not behave as a sensitizer in perovskite layer, but rather affect the properties of perovskite.

The overall enhancement of UV-Vis absorption is advantageous for the solar cell leading to an increased current density (J_{sc}) in device performance through wide range of solar lay in terms of wavelength. Based on the former studies reported by different groups, it can be elucidated that the increase of absorption band by additives attributed to dye molecules acting as defect passivator. [20]

We performed Photoluminescence (PL) measurement to elucidate how the D35CPDT dye affects the optoelectronic properties of the $MAPbI_3$ film. The perovskite layer was deposited on the glass without electron transporting layer (ETL) nor hole transporting layer (HTL) in order to evaluate the optoelectronic properties of the $MAPbI_3$ films itself. Figure 3.2.8 (a) shows significantly enhanced steady-state PL intensity of perovskite films with D35CPDT dye. Higher PL intensity confirms increase in the thickness of perovskite film with D35CPDT dye, which is consistent with the SEM images shown above. This result also imposes that D35CPDT dye can render perovskite films with reduced levels of non-radiative recombination on account of the absence of HTL and ETL. The wavelengths at maximum intensity were 766 nm for all three conditions. Therefore, there are no changes in band gap which can be proved from band gap plot from EQE in later section in Figure 3.3.1. The Time-Resolved PL (TRPL) decay is displayed in Figure 3.2.8 (b) and the related parameters are summarized in Table 3.2.1.

The TRPL was measured with the excitation at 766 nm for all three samples and characterized to investigate the influence of the enhanced crystallization of perovskite thin films on charge dissociation. In order to deeply investigate the dynamic differences from dye additives, the PL decay curves are fitted with bi-exponential function containing a fast

decay (τ_1) and a slow decay (τ_2) processes. [21] The fast decay component is derived from the quenching of free charge carriers through ETL or HTL, while the slow decay component is derived from the radiative recombination of free charge carriers before charge collection. It should be noted that the slow decay (τ_2) significantly increased from 49.904 ns with 86.05% ratio to 229.58 ns with 94.68% ratio and 157.388 ns with 98.68% ratio for perovskite film with LC dye and HC dye, respectively. This observation means that D35CPDT dye additive increases the intrinsic carrier lifetimes of the $MAPbI_3$ films and the depopulation of photo-induced charges was dominated by radiative recombination. However, the fraction of fast decay (τ_1) was very small and no meaningful difference between reference and two specimens with or without dye additive because there wasn't ETL nor HTL. Therefore, it can be concluded that the addition of dye can reduce the chance of non-radiative recombination caused by defects.

3.2.2 Physical Properties of the Perovskite films with and without D35CPDT

In order to determine if the absorption change was due to the existence of D35CPDT dye molecule in $MAPbI_3$ films, we performed the Time-of-Flight Secondary Ion Mass Spectrometry (ToF-SIMS). A full spectrum of the ToF-SIMS depth profile containing different elements was recorded and is shown in 3.2.3 (a-c). If not stated otherwise, the I^-, PbI_3^-, $CH_3CH_2I^-$, InO^-, SnO_2, OH^-, S^-, and $C_9HS_2^-$ intensity would be considered in our discussion for simplification. Compared with the reference film, the linker unit of D35CPDT dye molecule, cyclopentadithiophene, $C_9HS_2^-$, is only showed up in $MAPbI_3$ films with D35CPDT dye additives, Figure 3.2.3. (d-f). It is inevitable for the intensity of dye molecule to be very low since the concentration of D35CPDT molecules is significantly low compare to other detectable ions in $MAPbI_3$. Still, the existence and homogeneous distribution of D35CPDT molecules can be clearly observed from following

3D elemental mapping Figure 3.2.4, indicating that D35CPDT molecules are found in perovskite layer continuously. Moreover, given that D35CPDT contains anion charged functional groups that can passivate the positively charged or I^- vacancy in polycrystalline perovskite films [22], the D35CPDT dye might be able to form coordination with the positively charged under-coordinated Pb^{2+} ion or passivate the I^- vacancy in the perovskite film.

The thickness of $MAPbI_3$ with D35CPDT dye seems slightly higher than that of the reference perovskite in the feature of ToF-SIMS analysis. Some of ambiguity in elucidation of the ToF-SIMS depth profiling spectra is still refutable in terms of thickness measurement, because the sputtering time from SIMS measurement cannot be directly linked to the perovskite layer thickness as known previously. [22] However, the increased thickness for perovskite film with dye additive is also proved from following Scanning Electron Microscopy (SEM) images Figure 3.2.5.

To confirm the effect of D35CPDT dye molecule additive on thickness of perovskite, we conducted Scanning Electron Microscopy (SEM). Figure 3.2.5 (a-c) shows the cross-sectional SEM images of glass/ITO/Perovskite without and with D35CPDT dye additive of LC and HC. The thickness of the reference perovskite film is about 472 nm while the perovskite with LC dye and HL dye have thickness of 521 nm and 508 nm, respectively. Figure 3.2.5 (d-f) shows the top-view SEM images of perovskite films without and with LC dye and HC dye on ITO/glass substrates. The surface morphology of the perovskite films was significantly changed after the addition of small amount of D35CPDT dye. Whereas the reference $MAPbI_3$ film is covered with smaller sized grains Figure 3.2.5 (d), the $MAPbI_3$ films with D35CPDT additives exhibit relatively larger grain size. The grain sizes were also measured from surface images Figure 3.2.5 (d-f) of specimens fabricated at each condition by using Image J. The size range of the reference perovskite grain is from 55 nm to 394 nm with the average of 157 nm. The grain sizes of perovskite with the LC dye are from 96 nm to 929 nm with the average of 520 nm. The

grain sizes for the perovskite with HC dye also increased. The distributions of perovskite grain sizes obtained from SEM measurements are illustrated in Figure 3.2.6. The top-view SEM for lower magnification (Figure S3 a-c) also proves that the grain is enlarged from wider range. As a result, it is worth suggesting that the increased thickness of perovskite films with D35CPDT additive is simply ascribed not to increased amount of coated precursor but to enlarging grain size of perovskite. It possibly suggests that the different crystallization kinetics during the film formation via grain growth was led by dye additives. The cross-sectional SEM images also presented less grain boundary area, supporting that D35CPDT can facilitate the growth of high quality perovskite films.

X-ray diffraction (XRD) analysis was performed to evaluate the effect of D35CPDT on perovskite crystallinities Figure 3.2.7 (a) shows XRD patterns of perovskite film with and without D35CPDT dye. The diffraction peaks at 14.2, 28.5, and 31.9 for tetragonal MAPbI3 perovskite films can be indexed to the (110), (220), and (310) diffraction of perovskite grains, respectively. Compared to reference film, the absolute intensities of $MAPbI_3$ films with D35CPDT become stronger, implying that D35CPDT additive can improve the quantity and quality of perovskite grains. Figure 3.2.7 (b) displays the increased intensities of (110), (220), and (310) faces, meaning perovskite grain growth in all directions. The quality, such as crystallinity and the grain size, can be studied by observing FWHM values. The crystallite sizes calculated using Scherrer's equation (X), where τ is the mean crystallite size, λ is X-ray wave length, β is the FWHM values, and θ is the Bragg angle. Increased values of crystallite size (Å) as shown in Figure 3.2.7 (c) proves the grain size is increased in all directions. This observation is in agreement with the interpretation from SEM surface images (Figure 3.2.7).

Figure 1.

Figure 3.2.1. (a) Image of Perovskite precursor $MAPbI_3$ solution and perovskite with dyes molecule additives ($6.0e^{-5}$M), (b) Dye Stocks (D35CPDT), (c) UV-Vis absorption spectra of control film and Dye MAPbI3 mixture films.

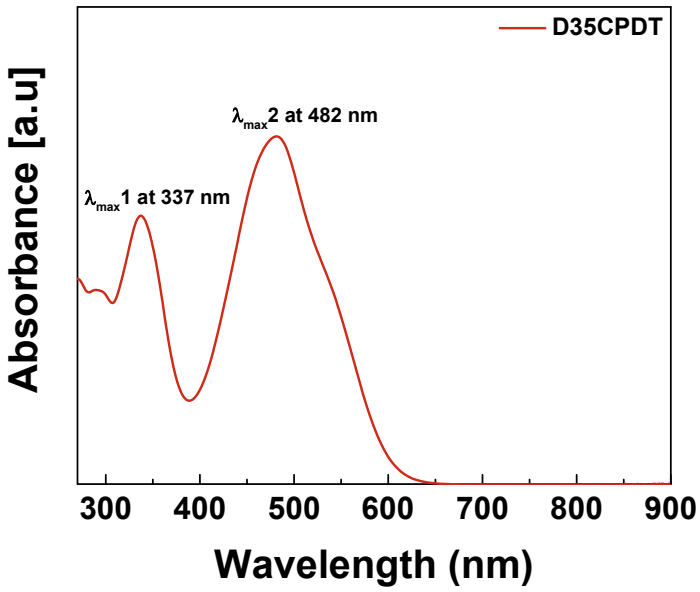

Figure 3.2.2. UV-Vis absorption spectra of D35CPDT in DMF: DMSO solvent

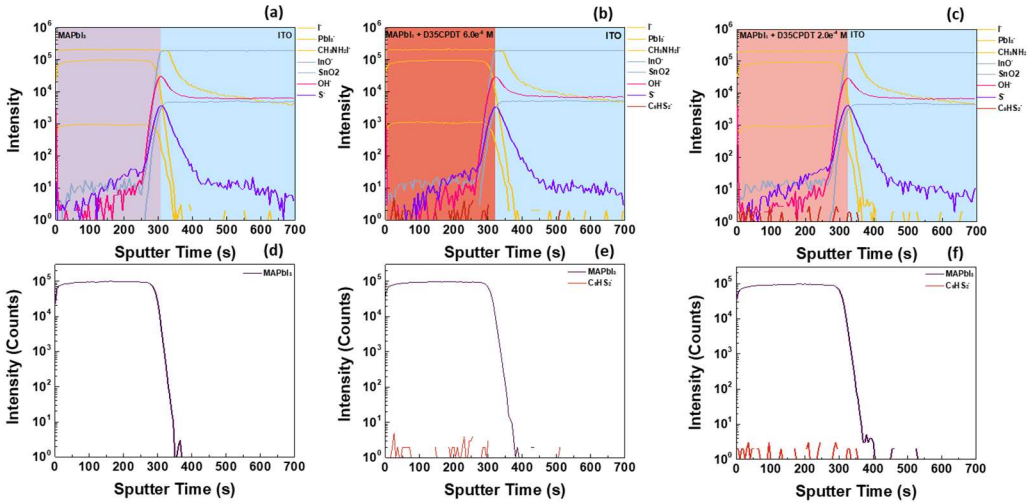

Figure 3.2.3. Visualized depth profiles of (a)(d) reference perovskite film, (b)(e) $MAPbI_3$ with LD dye, and (c)(f) $MAPbI_3$ with HC dye.

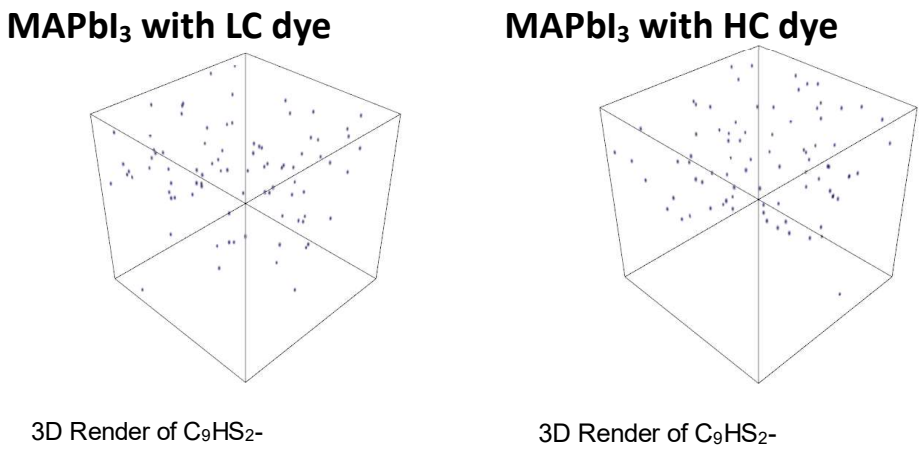

Figure 3.2.4. 3D image of ToF-SIMS depth profiling of $C_9HS_2^-$ molecule.

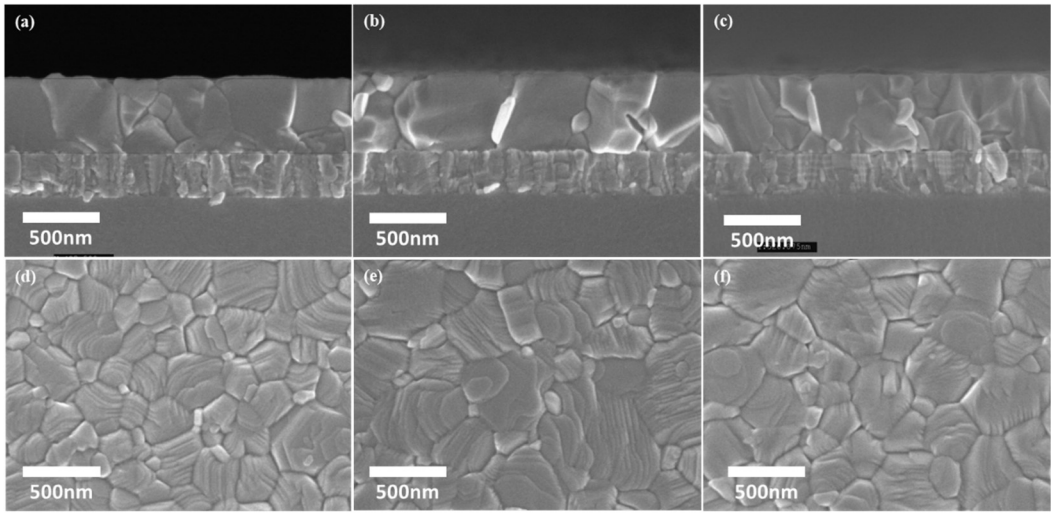

Figure 3.2.5. (Top) Cross-section SEM images of (a) reference perovskite film on ITO/glass, and (b)(c) Perovskite with D35CPDT dye of $6.0e^{-5}$M and $2.0e^{-4}$M, respectively. (Bottom) Top-view SEM images of (d) control perovskite film on ITO/glass, and (e)(f) Perovskite with D35CPDT dye of $6.0e^{-5}$M and $2.0e^{-4}$M, respectively.

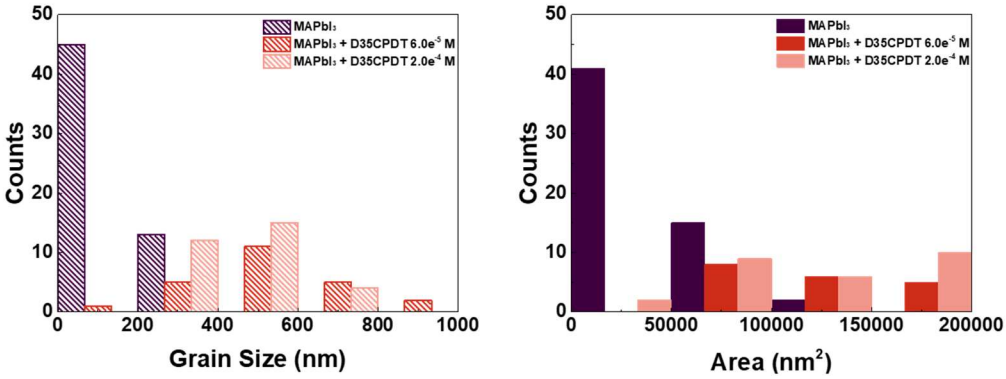

Figure 3.2.6. Histogram of the diameters (denoted as grain sizes) and the area of perovskite grains measure by Image J for each conditions.

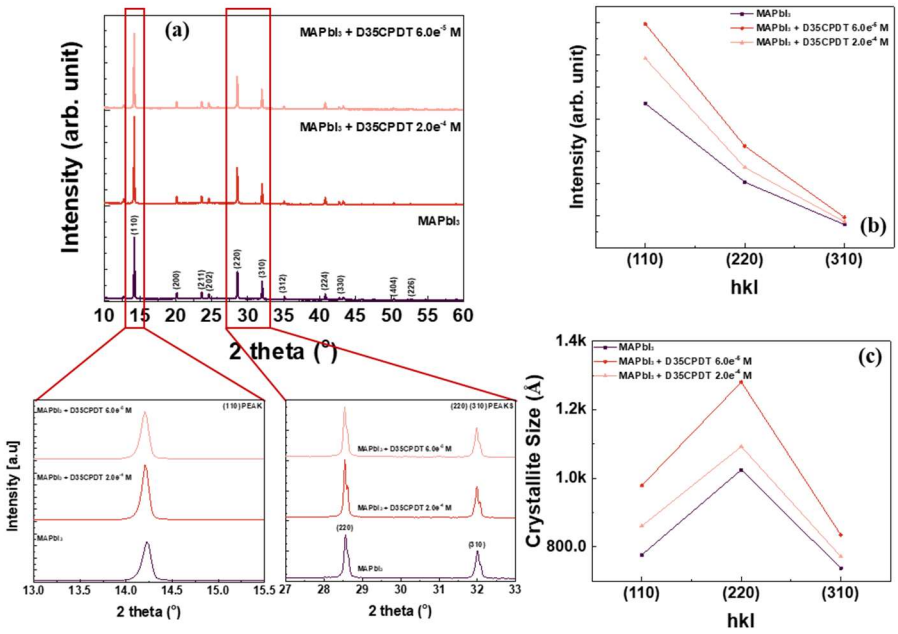

Figure 3.2.7. (a) XRD patterns for $MAPbI_3$ reference perovskite film and $MAPbI_3$ perovskite films containing D35CDT dye with LC dye and HC dye. The magnified graph exhibits the main peaks of $MAPbI_3$. (b) Intensity of $MAPbI_3$ main peaks in arbitrary units. (c) Calculated crystallite size (Å) the full width at half maximum (FWHM) using Scherrer's Equation.

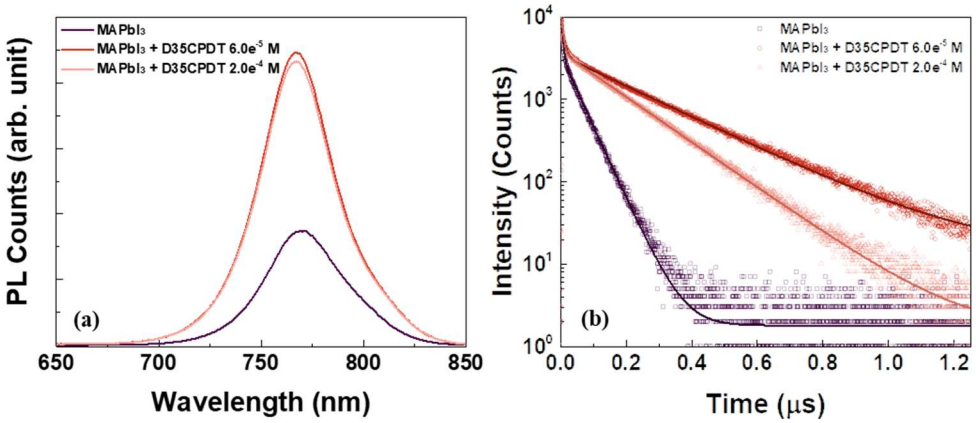

Figure 3.2.8. (a) Steady-State and (b) Time-Resolved PL spectra of the perovskite layer with two LC dye and HC dye of dyes on glass substrate.

Perovskite Composition	τ_1 (ns)	Fraction 1	τ_2 (ns)	Fraction 2
REF	4.093	13.95%	49.904	86.05 %
D35CPDT 6.0e^{-5} M (LC)	8.172	5.32 %	229.58	94.68 %
D35COPDT 2.0e^{-4} M (HC)	5.665	5.32 %	157.388	94.68 %

Table 3.2.1. Time resolved photoluminescence characterization of the perovskite with and without D35CPDT molecule additives on glass.

3.3 Device Characterization

3.3.1 Performance and Electron Dynamics of perovskite solar cell

To investigate effect of the addition of D35CPDT dye on the device performances, we fabricated the perovskite solar cells with and without D35CPDT dye. The structure of the perovskite solar cells is glass/ITO/NiO/$MAPbI_3$/$PC_{60}BM$/PEIE/Ag as displayed in inset of the Figure 3.3.1. Figure 3.3.1 shows *J-V* curves of perovskite solar cells with average performances and each parameters are summarized in **Table 2**. The short-circuit current density (J_{sc}) for reference, LC dye, and HC dye cells were 21.06 mA cm^{-2}, 22.01 mA cm^{-2} and 21.67 mA cm^{-2}, respectively. This increase in the J_{sc} can be ascribed to increased absorption shown above and also identified from the integrated J_{sc} values calculated by external quantum efficiency (EQE) measurement (Figure 3.3.1 (b)). The open-circuit voltage (V_{oc}) with average value is barely influenced by the addition of the D35CPDT dye. Considering that there was no change in band-gap in perovskite films with LC and HC dye, indicating that D35CPDT molecule is not acting as sensitizer, this result is acceptable. The fill factor for reference, LC dye, and HC dye cells were 0.80, 0.81, and 0.80, respectively. The photo conversion efficiency (PCE) for reference, LC dye, and HC dye cells were 17.48 %, 18.56 %, and 18.07 %, respectively. The improved performances can be clearly observed by the statistics presented in Figure 3.3.2. As a results, the improved efficiency was mainly contributed from the increase in J_{sc}, which can be ascribed to the high-quality perovskite by the addition of D35CPDT dye. Furthermore, electrochemical impedance spectroscopy (EIS) shows the same trend with analysis above. The EIS measurement was performed in the open-circuit condition with the light illumination (white LED) showing a V_{oc} value. The Nyquist plot shows increased size of the arc in the high-frequency range with D35CPDT dye Figure 3.3.1 (c), which can be

ascribed to the increase in recombination resistance of the perovskite solar cell with the dye additives. [23] The bode plot shows the imaginary part of the impedance plotted as a function of frequency Figure 3.3.1 (d). Compared to reference solar cell, the decreased frequency of the peak with D35CPDT dye indicates increased carrier lifetime through the following equation: $\tau=1/\omega c=1/2\pi fc$, where τ is the lifetime, ωc is the characteristic radial frequency, and fc is the characteristic frequency. [24] As a result, this observation is in agreement with the interpretation from the previous analysis and observations from measurements.

3.3.2 Stability

As mentioned in the introduction, D35CPDT molecules are consisted with multiple long alkyl chains, which can affect the stability of the perovskite solar cells. [25] In order to see if the addition of D35CPDT dye would enhance stability of the perovskite solar cells, the devices were kept under a controlled RH of under 40% at the temperature of 25 °C under ambient without encapsulation. Figure 3.3.3 compares the stability of the perovskite solar cell as a function of addition of D35CPDT dye. The J_{sc} and the V_{oc} of perovskite solar cell with dye additives were remained more than 80% of their initial values after being exposed to ambient for 650 hours. On the other hand, both parameters of reference devices were dropped to 0%. The fill factor of perovskite solar cell with dye additives was also remained over 60%, however, that of reference device dropped to 60% after 350 hours and 0% after 650 hours. The degradation of PCE can be mainly ascribed to the continuous decrease in J_{sc} and Fill factor. Therefore, it can be concluded that the addition of D35CPDT dye can enhance the performance of the perovskite solar cell and also improve the device stability as intended.

As mentioned hereinbefore, the dye seems to play a benign role in the fabrication process of perovskite solar cell. The proper amount of dye additives is favorable to obtain

perovskite solar cell with advantages of a grain dimension and a lower trap density. Further studies including optimization of dye structure and concentration etc. can show a new way to improve the performance of perovskite solar cell.

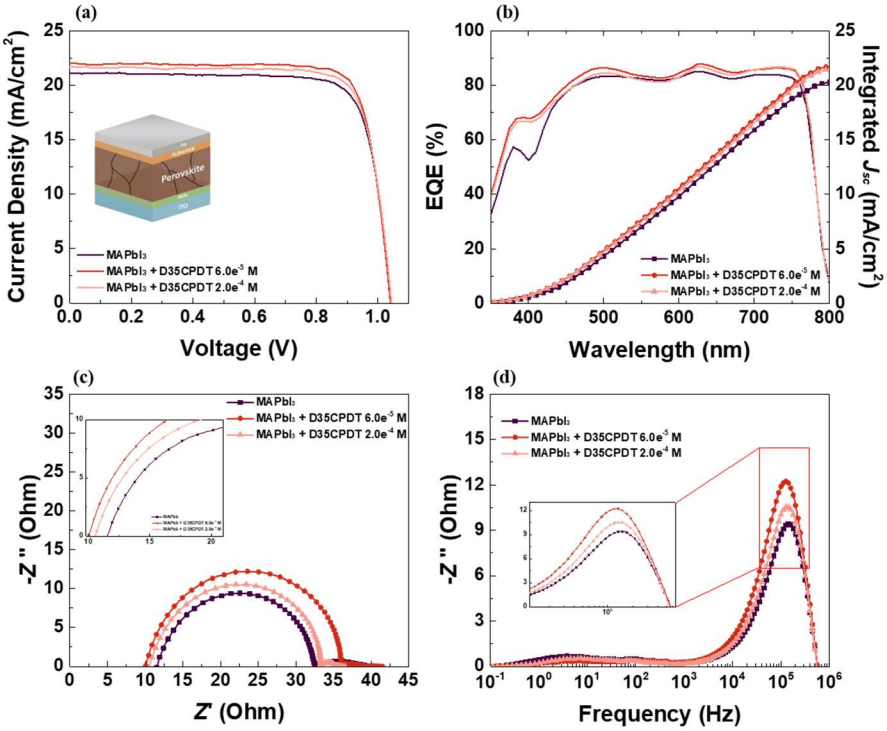

Figure 3.3.1. (a) J-V curve of perovskite photovoltaic devices with and without LC dye and HC dye additive. The inset indicates the overall architecture of the device and fabrication method is mentioned in Experimental section, (b) EQE analysis, (c) Nyquist Plots, and (d) –Z" versus frequency plot

Perovskite Composition		EQE J_{sc} (mA cm^{-2})	J_{sc} (mA cm^{-2})	V_{oc} (V)	PCE (%)	FF
$MAPbI_3$	Average	20.30	21.06	1.04	17.48	0.80
	Champion	-	22.04	1.03	18.46	0.81
D35CPDT 6.0e^{-5} M	Average	21.75	22.01	1.04	18.56	0.81
	Champion	-	22.34	1.05	19.17	0.82
D35CPDT 2.0e^{-4} M	Average	21.48	21.67	1.04	18.07	0.80
	Champion	-	21.55	1.06	18.64	0.82

Table 3.3.1 Solar Cell Performance Parameters of $MAPbI_3$ perovskite devices with and with LC dye and HC dye.

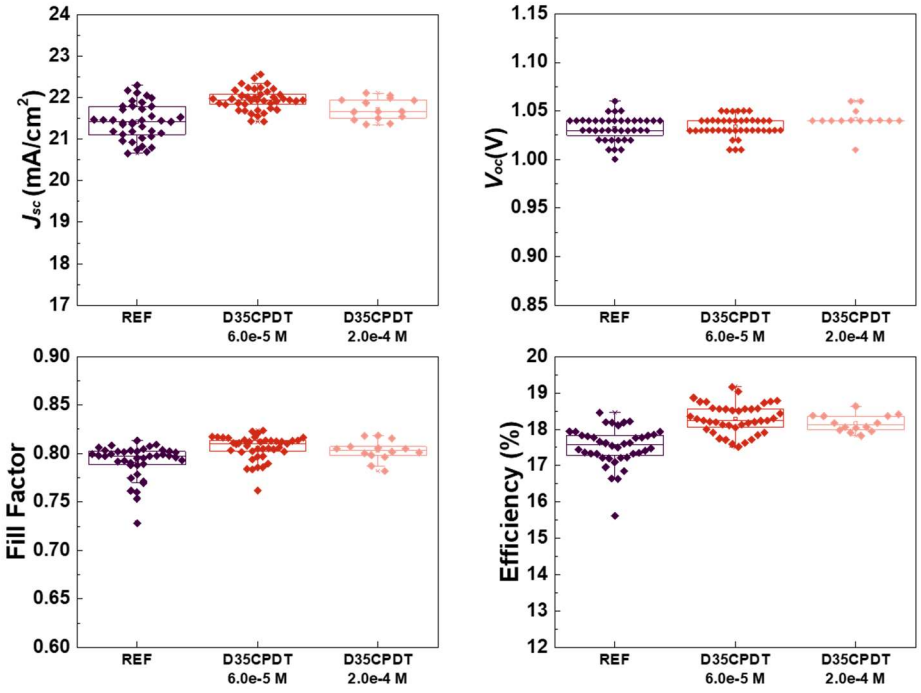

Figure 3.3.2. Box plot of each solar cells for perovskite reference device and perovskite with LC dye and HC dye.

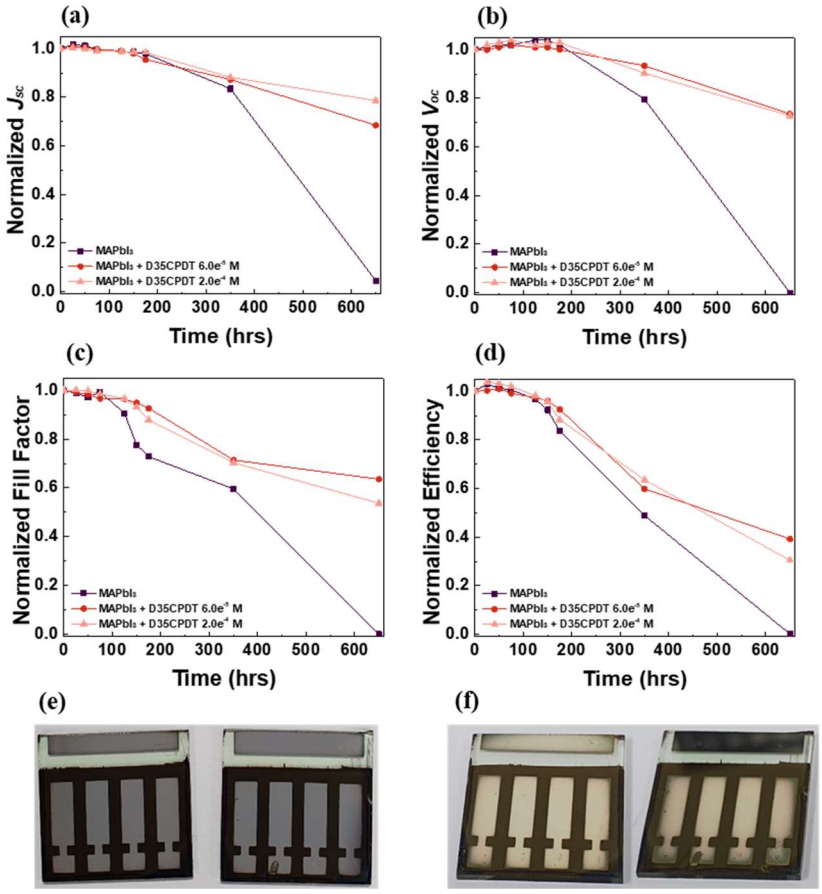

Figure 3.3.3. Stability. The variation of four normalized photovoltaic performance parameters: (a) J_{sc}, (b) V_{oc}, (c) Fill factor, and (d) Efficiency (%). All of the devices were kept under ambient conditions (temperature of 25°C; humidity of 40%). (e-f) Device on the left is $MAPbI_3$ with LC dye and that on the right is reference. (e) Photograph of devices taken on the day of fabrication, and (f) photograph of devices after 650 hours kept under ambient.

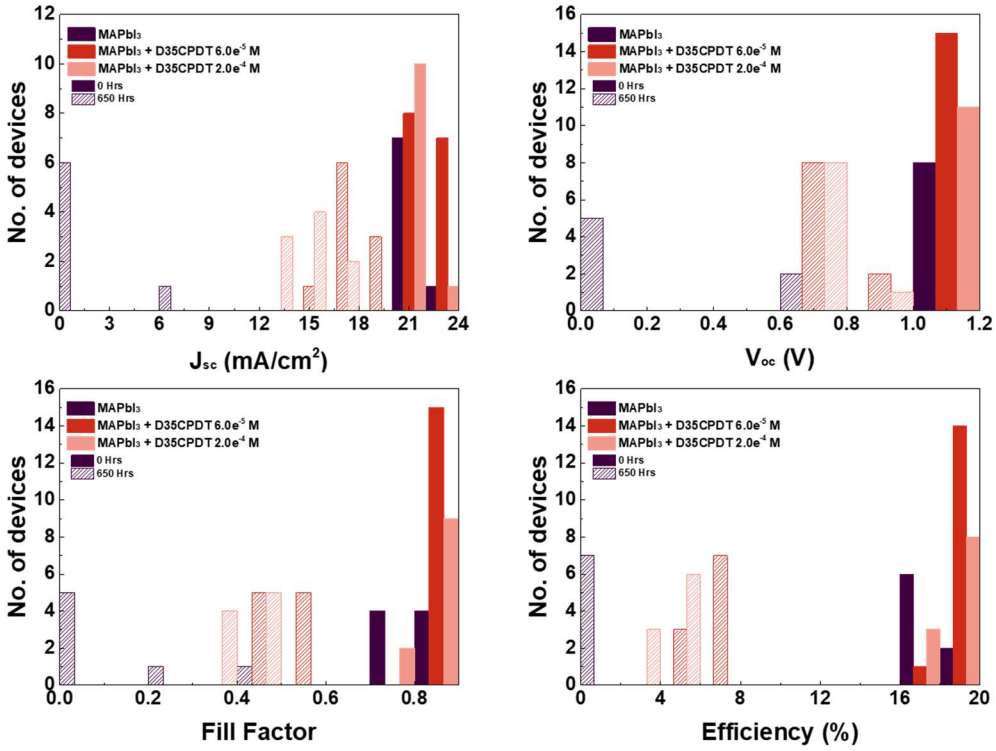

Figure 3.3.4. Histogram of device performance distribution on perovskite devices with and without D35CPDT molecule additive from 0 h to 650 h.

Chapter 4. Conclusion

We investigated the improved properties of $MAPbI_3$ perovskite through D35CPDT molecule additive. The analysis from XRD and SEM images of $MAPbI_3$ with D35CPDT additives obviously shows the enlarged grain sizes and (increased) crystallinity compared to the reference $MAPbI_3$ films. Not only with the those numerical and visible results, the existence of D35CPDT molecules was also proved by ToF-SIMS analysis. Therefore, we can conclude that the D35CPDT molecules coordinate to the metal cations, passivating the I- vacancy, the critical cause of perovskite deterioration. PL measurements also show the remarkably delay in lifetime of the charge carriers in perovskite layer with additives. This indicates that the charge carriers in $MAPbI_3$ film with D35CPDT molecules tend to recombine at slower rate compare to reference film. The EIS measurements also exhibit that the carrier lifetime of the perovskite solar cells with additive is increased. These observations support our expectation that negatively charged functional group in D35CPDT molecule can passivate the metal cation and reduce defect sites. The D35CPDT molecule additives were studied with two different concentrations; $6.0\ e^{-5}$ M and $2.0\ e^{-4}$ M. The results with both concentrations show enhanced properties of $MAPbI_3$ films and performance of $MAPbI_3$ perovskite solar cells. However, slight decrease of all properties were observed, as the concentration of D35CPDT increased. As a result, the improvement reaches the maximum when proper amount of D35CPDT additives is added. At last, the outstanding enhancement in crystallization caused by addition of D35CPDT are responsible for improved stability of the solar cells.

Bibliography

[1] NREL Efficiency chart, https://www.nrel.gov/pv/cell-efficiency.html#.XaAyyyyKrwo.link).

[2] N. Ahn, D. Y. Son, I. H. Jang, S. M. Kang, M. Choi and N. G. Park, J Am Chem Soc, 2015, 137, 8696-8699.

[3] G. A. Al-Dainy, S. E. Bourdo, V. Saini, B. C. Berry and A. S. Biris, Energy Technology, 2017, 5, 373-401.

[4] G. A. Al-Dainy, S. E. Bourdo, V. Saini, B. C. Berry and A. S. Biris, Energy Technology, 2017, 5, 373-401.

[5] C. Besleaga, L. E. Abramiuc, V. Stancu, A. G. Tomulescu, M. Sima, L. Trinca, N. Plugaru, L. Pintilie, G. A. Nemnes, M. Iliescu, H. G. Svavarsson, A. Manolescu and I. Pintilie, J Phys Chem Lett, 2016, 7, 5168-5175.

[6] F. Cai, Y. Yan, J. Yao, P. Wang, H. Wang, R. S. Gurney, D. Liu and T. Wang, Advanced Functional Materials, 2018, 28.

[7] B. Chen, H. Hu, T. Salim and Y. M. Lam, Journal of Materials Chemistry C, 2019, 7, 5646-5651.

[8] Y. Chen, N. Li, L. Wang, L. Li, Z. Xu, H. Jiao, P. Liu, C. Zhu, H. Zai, M. Sun, W. Zou, S. Zhang, G. Xing, X. Liu, J. Wang, D. Li, B. Huang, Q. Chen and H. Zhou, Nat Commun, 2019, 10, 1112.

[9] Z. Chu, M. Yang, P. Schulz, D. Wu, X. Ma, E. Seifert, L. Sun, X. Li, K. Zhu and K. Lai, Nat Commun, 2017, 8, 2230.

[10] J.-P. Correa-Baena, A. Abate, M. Saliba, W. Tress, T. Jesper Jacobsson, M.

Grätzel and A. Hagfeldt, Energy & Environmental Science, 2017, 10, 710-727.

[11] J.-P. Correa-Baena, W. Tress, K. Domanski, E. H. Anaraki, S.-H. Turren-Cruz, B. Roose, P. P. Boix, M. Grätzel, M. Saliba, A. Abate and A. Hagfeldt, Energy & Environmental Science, 2017, 10, 1207-1212.

[12] H. Ellis, S. K. Eriksson, S. M. Feldt, E. Gabrielsson, P. W. Lohse, R. Lindblad, L. Sun, H. Rensmo, G. Boschloo and A. Hagfeldt, The Journal of Physical Chemistry C, 2013, 117, 21029-21036.

[13] P. Fassl, Y. Zakharko, L. M. Falk, K. P. Goetz, F. Paulus, A. D. Taylor, J. Zaumseil and Y. Vaynzof, Journal of Materials Chemistry C, 2019, 7, 5285-5292.

[14] E. Gabrielsson, H. Ellis, S. Feldt, H. Tian, G. Boschloo, A. Hagfeldt and L. Sun, Advanced Energy Materials, 2013, 3, 1647-1656.

[15] Q. Han, Y. Bai, J. Liu, K.-z. Du, T. Li, D. Ji, Y. Zhou, C. Cao, D. Shin, J. Ding, A. D. Franklin, J. T. Glass, J. Hu, M. J. Therien, J. Liu and D. B. Mitzi, Energy & Environmental Science, 2017, 10, 2365-2371.

[16] L. M. Herz, ACS Energy Letters, 2017, 2, 1539-1548.

[17] X. Hou, S. Huang, W. Ou-Yang, L. Pan, Z. Sun and X. Chen, ACS Appl Mater Interfaces, 2017, 9, 35200-35208.

[18] J. Huang, Y. Yuan, Y. Shao and Y. Yan, Nature Reviews Materials, 2017, 2.

[19] M. Jahandar, N. Khan, H. K. Lee, S. K. Lee, W. S. Shin, J. C. Lee, C. E. Song and S. J. Moon, ACS Appl Mater Interfaces, 2017, 9, 35871-35879.

[20] N. J. Jeon, J. H. Noh, Y. C. Kim, W. S. Yang, S. Ryu and S. I. Seok, Nat Mater,

2014, 13, 897-903.

[21] S. S. Juang, P. Y. Lin, Y. C. Lin, Y. S. Chen, P. S. Shen, Y. L. Guo, Y. C. Wu and P. Chen, Front Chem, 2019, 7, 209.

[22] E. J. Juarez-Perez, L. K. Ono, M. Maeda, Y. Jiang, Z. Hawash and Y. Qi, Journal of Materials Chemistry A, 2018, 6, 9604-9612.

[23] A. Kaltzoglou, D. Perganti, M. Antoniadou, A. G. Kontos and P. Falaras, Energy Procedia, 2016, 102, 49-55.

[24] H.-S. Kim, C.-R. Lee, J.-H. Im, K.-B. Lee, T. Moehl, A. Marchioro, S.-J. Moon, R. Humphry-Baker, J.-H. Yum, J. E. Moser, M. Grätzel and N.-G. Park, Scientific Reports, 2012, 2, 591.

[25] A. Kogo, T. Miyadera and M. Chikamatsu, ACS Appl Mater Interfaces, 2019, 11, 38683-38688.

[26] C. Li, A. Wang, L. Xie, X. Deng, K. Liao, J.-a. Yang, T. Li and F. Hao, Journal of Materials Chemistry A, 2019, 7, 24150-24163.

[27] D. Li, P. Liao, X. Shai, W. Huang, S. Liu, H. Li, Y. Shen and M. Wang, RSC Advances, 2016, 6, 89356-89366.

[28] X. Li, C.-C. Chen, M. Cai, X. Hua, F. Xie, X. Liu, J. Hua, Y.-T. Long, H. Tian and L. Han, Advanced Energy Materials, 2018, 8.

[29] Y. Li, L. Meng, Y. M. Yang, G. Xu, Z. Hong, Q. Chen, J. You, G. Li, Y. Yang and Y. Li, Nat Commun, 2016, 7, 10214.

[30] P. W. Liang, C. Y. Liao, C. C. Chueh, F. Zuo, S. T. Williams, X. K. Xin, J. Lin and A. K. Jen, Adv Mater, 2014, 26, 3748-3754.

[31] D. Meggiolaro, E. Mosconi and F. De Angelis, ACS Energy Letters, 2019, 4, 779-785.

[32] C. Motta, F. El-Mellouhi, S. Kais, N. Tabet, F. Alharbi and S. Sanvito, Nat Commun, 2015, 6, 7026.

[33] W. Nie, H. Tsai, R. Asadpour, J.-C. Blancon, A. J. Neukirch, G. Gupta, J. J. Crochet, M. Chhowalla, S. Tretiak, M. A. Alam, H.-L. Wang and A. D. Mohite, Science, 2015, 347, 522.

[34] B. W. Park, N. Kedem, M. Kulbak, D. Y. Lee, W. S. Yang, N. J. Jeon, J. Seo, G. Kim, K. J. Kim, T. J. Shin, G. Hodes, D. Cahen and S. I. Seok, Nat Commun, 2018, 9, 3301.

[35] S. R. Raga, Y. Jiang, L. K. Ono and Y. Qi, Energy Technology, 2017, 5, 1750-1761.

[36] J. M. Remington, A. M. Philip, M. Hariharan and B. Kohler, The Journal of Chemical Physics, 2016, 145, 155101.

[37] Y. Shao, Z. Xiao, C. Bi, Y. Yuan and J. Huang, Nat Commun, 2014, 5, 5784.

[38] D.-Y. Son, J.-W. Lee, Y. J. Choi, I.-H. Jang, S. Lee, P. J. Yoo, H. Shin, N. Ahn, M. Choi, D. Kim and N.-G. Park, Nature Energy, 2016, 1.

[39] S. D. Stranks, G. E. Eperon, G. Grancini, C. Menelaou, M. J. Alcocer, T. Leijtens, L. M. Herz, A. Petrozza and H. J. Snaith, Science, 2013, 342, 341-344.

[40]. W.-Y. Tan, P.-P. Cheng, Y.-W. Zhang, J.-M. Liang, X. Chen, Y. Liu and Y. Min, Journal of Materials Chemistry C, 2019, 7, 6004-6011.

[41] S.-H. Turren-Cruz, A. Hagfeldt and M. Saliba, Science, 2018, 362, 449.

[42] J. Wei, Y. Zhao, H. Li, G. Li, J. Pan, D. Xu, Q. Zhao and D. Yu, J Phys Chem Lett, 2014, 5, 3937-3945.

[43] L. D. Whalley, J. M. Frost, Y. K. Jung and A. Walsh, J Chem Phys, 2017, 146, 220901.

[44] Z. Xiao, Q. Dong, C. Bi, Y. Shao, Y. Yuan and J. Huang, Adv Mater, 2014, 26, 6503-6509.

[45] Y. Xie, J. Baillargeon and T. W. Hamann, The Journal of Physical Chemistry C, 2015, 119, 28155-28166.

[46] G. Xing, N. Mathews, S. Sun, S. S. Lim, Y. M. Lam, M. Gratzel, S. Mhaisalkar and T. C. Sum, Science, 2013, 342, 344-347.

[47] D. Yang, R. Yang, J. Zhang, Z. Yang, S. Liu and C. Li, Energy & Environmental Science, 2015, 8, 3208-3214.

[48] M. Yang, D. H. Kim, Y. Yu, Z. Li, O. G. Reid, Z. Song, D. Zhao, C. Wang, L. Li, Y. Meng, T. Guo, Y. Yan and K. Zhu, Materials Today Energy, 2018, 7, 232-238.

[49] H. Yoon, S. M. Kang, J.-K. Lee and M. Choi, Energy & Environmental Science, 2016, 9, 2262-2266.

[50] J. You, Y. Yang, Z. Hong, T.-B. Song, L. Meng, Y. Liu, C. Jiang, H. Zhou, W.-H. Chang, G. Li and Y. Yang, Applied Physics Letters, 2014, 105.

[51] Y. Yuan and J. Huang, Acc Chem Res, 2016, 49, 286-293.

[52] M. Zhang, M. Tai, X. Li, X. Zhao, H. Chen, X. Yin, Y. Zhou, Q. Zhang, J. Han, N. Wang and H. Lin, Solar RRL, 2019, 3, 1900345.

[53] T. Zhang, X. Meng, Y. Bai, S. Xiao, C. Hu, Y. Yang, H. Chen and S. Yang, Journal of Materials Chemistry A, 2017, 5, 1103-1111.

[54] Y. Zhao, A. M. Nardes and K. Zhu, J Phys Chem Lett, 2014, 5, 490-494.

[55] Y. Zhao, W. Zhou, W. Ma, S. Meng, H. Li, J. Wei, R. Fu, K. Liu, D. Yu and Q. Zhao, ACS Energy Letters, 2016, 1, 266-272.

Abstract in Korean

국문 초록

유-무기 할라이드 페로브스카이트 태양전지는 최근 최고 효율의 25%를 도달하며, Shockley-Queisser 한계 효율에 다가가기위해 활발한 연구가 진행되고 있다. 그러나, 페로브스카이트 태양전지의 안정성 문제는 여전히 해결되지않고 꾸준이 문제가 제기되고 있다. 이러한 만족스럽지 못한 안정성은 주로 페로브스카이트층의 이온성 결함으로 인해 불안정하고 열악한 결정성이 원인이며, 첨가제 조절을 통해 문제를 해결하고자 하는 연구가 많이 진행되고 있다. 다양한 첨가제들 중, 염료 분자 첨가제는 치환기, 특히 음전하를 띄는 작용기를 가지고 있으며 이 작용기는 요오드 결함에 의해 야기된 금속 양이온 결함과 조합되어 결함을 패시베이션 시킬 수있다.

본 연구에서는 페로브스카이트 태양전지의 용액 공정에서, D35CPDT 염료 분자 첨가제를 MAPbI3 페로브스카이 전구물질에 첨가하여 페로브스카이트 박막 자체의 속성을 향상시키고, 소자 성능의 증가를 확인하였다. D35CPDT 분자의 첨가에 의해 페로브스카이트 박막에서의 입자의 크기, 결정석, 그리고 광흡수량등이 증가하였다. 이러한 향상으로 전류밀도 (*J*sc)가 21.06 mA cm^{-2}에서 22.06 mA cm^{-2}로 증가하여 전력 변환 효율이 17.48 %에서 18.56 %로 증가함을 증명하였다. 또한 염료 첨가제 사용에 의한 태양전지 소자의 안정성 향상도 확인하였다. D35CPDT 분자 첨가제가 포함 된 MAPbI3의 전류밀도 (J_{sc}) 및 개방회로전압 (V_{oc})은 별도의 보호처리 없이 실온에서 650 시간 보관하였을 경우 80% 이상을 유지한 반면, 첨가제가 들어가지

않은 페로브스카이트 샘플은 650시간 후에 0%로 떨어졌다. 이러한 결과는 작용기 및 알킬기를 갖는 큰 분자의 첨가가 페로브스카이트의 결정화 특성을 개선 할뿐만 아니라 장치의 수명을 연장시킬 수 있다는 것을 증명할 수 있다.

주요어: 페로브스카이트 태양전지, 용액 공정, 첨가제 엔지니어링, 염료감응태양전지

학 번: 2018-29417